High Magnetic Moments in Manganese Doped Silicon Clusters

Vu Thi Ngan,[a,*] Ewald Janssens,[b] Pieterjan Claes,[b] Jonathan T. Lyon,[c] André Fielicke,[d,*] Minh Tho Nguyen,[a] and Peter Lievens[b,*]

[a] *Department of Chemistry, KU Leuven, B-3001 Leuven, Belgium*

[b] *Laboratory of Solid State Physics and Magnetism, KU Leuven, B-3001 Leuven, Belgium*

[c] *Department of Natural Sciences, Clayton State University, Morrow, Georgia 30260, USA*

[d] *Fritz-Haber-Institut der Max-Planck-Gesellschaft, D-14195 Berlin, Germany*

---

*Emails: thingan.vu@chem.kuleuven.be, fielicke@fhi-berlin.mpg.de, peter.lievens@fys.kuleuven.be

---

Version 25 May 2012

(ABSTRACT) We report on the structural, electronic, and magnetic properties of manganese-doped silicon clusters cations, Si_nMn^+ with $n = 6-10$, 12−14 and 16, using mass spectrometry and infrared spectroscopy in combination with density functional theory computations. This combined experimental and theoretical study allows several structures to be identified. All the exohedral Si_nMn^+ (n = 6−10) clusters are found to be substitutive derivatives of the bare Si_{n+1}^+ cations, while the endohedral Si_nMn^+ (n = 12−14 and 16) clusters adopt fullerene-like structures. The hybrid B3P86 functional is shown to be appropriate in predicting the ground electronic states of the clusters and in reproducing their infrared spectra. The clusters turn out to have high magnetic moments localized on Mn. In particular the Mn atoms in the exohedral Si_nMn^+ (n = 6−10) clusters have local magnetic moments of 4 μ_B or 6 μ_B and can be considered as magnetic copies of the silicon atoms. Opposed to other 3d transition metal dopants, the local magnetic moment of the Mn atom is not completely quenched when encapsulated in a silicon cage.

KEYWORDS: Mn-doped silicon clusters, infrared spectroscopy, local magnetic moments, magnetic building blocks

1. Introduction

Silicon has been and continues to be one of the most widely used elements in various semiconductor applications such as solar cells and microelectronics. Consequently, the chemical and physical properties of nanometer-sized silicon species have intensively been studied for several decades.[1,2] Nonetheless, the structures of some small clusters, such as Si_8^+, could only recently be established by combined experimental and theoretical work.[3]

Incorporation of transition metal (TM) dopant atoms into silicon clusters constitutes a promising way for tailoring the optoelectronic properties and the stability of clusters.[4,5] Many elements from all the groups of the Periodic Table have been considered as dopants.[6-15] Doping with atoms that have only partially filled *d* or *f* shells that can carry a magnetic moment may be a way to realize magnetic nanometer sized silicon particles. This is of particular interest for a wide range of applications, including in magnetic fluids, biotechnology, magnetic resonance imaging, and data storage.[16] Most importantly, the potential applications of spin-based electronic devices urge more research on magnetic semiconductors.[17] It was shown that lanthanide atoms may retain a significant part of their atomic magnetic moment when embedded in a silicon cage due to the limited involvement of the 4*f*-electrons in the bonding with Si atoms.[18] However upon impregnation of a silicon cluster with a magnetic 3*d* transition metal atom, the strong interaction of the silicon *s*- and *p*-orbitals with the *d*-orbitals of the TM atom is calculated to largely quench the latter's magnetic moment from a small size onwards, such as for Si_nCr ($n \geq 8$),[19,20] Si_nFe ($n \geq 9$),[21] Si_nCo ($n \geq 7$),[22] and Si_nNi ($n \geq 3$).[23]

When encapsulated in a Si cage, the local magnetic moment of the TM dopant is often quenched such as in $V@Si_n^+$ (n = 12−16) clusters.[24] Even with magnetic elements, theoretical studies, e.g. for $TM@Si_{12}$ with TM = Cr, Mn, Fe, Co, and Ni,[25-27] predicted that the TM-doped silicon clusters are in the lowest spin state possible. On the other hand, Singh *et al.*[27] predicted that the magnetic properties of TM-doped silicon nanotubes, constructed from hexagonal prism building blocks, may be tuned by

selecting the appropriate dopants. In particular Fe and Mn atoms show high local magnetic moments in finite silicon nanotubes, whereas Co has rather low corresponding values and Ni doped silicon nanotubes are not magnetic at all. It has recently been proposed that the magnetic moments may be recovered if two non-magnetic $Si_{12}Cr$ clusters are brought together.[28] Unfortunately, there is no experimental information on magnetic properties of doped silicon cluster so far to verify these theoretical predictions.

Of the 3*d* TMs, the Mn atom which in its ground state is characterized by the half-filled 3*d* shell and a filled 4*s* shell, has a particularly large magnetic moment of 6 μ_B. As a matter of fact, manganese is one of the most complex magnetic elements because of its special spin coupling behavior. For example while the neutral Mn_2 dimer has an antiferromagnetic coupling in its singlet ground state, a ferromagnetic coupling has been found for the high spin ground state of the Mn_2^+ cation.[29] The magnetic properties of Mn-based materials are supposed to relate to the maximum number of unpaired electrons in the 3*d* shell of the Mn^+ cation[30] or the Mn^{2+} dication.[31] Nonetheless, already in the early 1960's, it became clear that upon doping silicon crystals with Mn, in both substitutional and interstitial sites, the Mn atoms carry only small magnetic moments.[32]

Low spin ground states were recently predicted for small neutral clusters Si_nMn by density functional theory (DFT) computations using the PW91 method, a popular pure GGA functional.[33] This result is however not confirmed in the present combined experimental and theoretical study on the small cationic manganese doped silicon clusters of which the Mn atom carries large local magnetic moments. Here we report on the structural, electronic, and magnetic properties of cationic Si_nMn^+ clusters with $n = 6-10$, $12-14$ and 16. The ground state structures of the clusters are identified using infrared spectroscopy on the cluster−rare gas complexes in combination with quantum chemical calculations based on DFT methods.

2. Methods

A. Experimental Setup

The experiments are performed in a molecular beam setup, which contains a dual laser vaporization source[34] and a time-of-flight mass spectrometer equipped for infrared (IR) excitation experiments.[35] The setup is connected to a beamline of the Free Electron Laser for Infrared eXperiments (FELIX) at the FOM Institute for Plasma Physics 'Rijnhuizen' in Nieuwegein, the Netherlands.[36] The source parameters are optimized for the formation of cold singly manganese doped silicon clusters. Rare gas atoms, which act as messenger atoms,[37] are attached to the clusters to record the IR spectra of the clusters in the gas phase. The formation of cluster–argon (at 100 K) and cluster–xenon (at 120 K) complexes is induced by addition of a fraction of 1% of Ar or of 0.5% of enriched ^{129}Xe to the He carrier gas, respectively. Resonant absorption of IR photons and subsequent vibrational energy redistribution heat the clusters and may result in evaporation of the weakly bound rare gas atom. The IR multiple photon dissociation (IRMPD) spectra are constructed by recording the ion intensities of the cluster−rare gas complexes as a function of the FELIX frequency in the 230−500 cm^{-1} (for Si_nMn^+·Xe) and 250−550 cm^{-1} (for Si_nMn^+·Ar) ranges. From the depletion spectra, IR absorption spectra are calculated as described previously.[35] Xe could be used as a messenger atom for all cluster sizes while Ar could be only utilized for small sizes (n < 11) but Si_7Mn^+. A detailed analysis of the special behavior of Si_7Mn^+ will be carried out in a future study.

B. Theoretical Methods

The vibrational spectra are unique structural fingerprints of the clusters and therefore structural identification is possible upon comparison with simulated spectra that result from detailed quantum-chemical computations. DFT is currently an unrivaled theoretical tool for the treatment of clusters containing transition metals. However, application of DFT does require a proper choice of the functional, since none of the broad variety of functionals developed so far adequately describes all

properties of a type of compounds. For example, the pure BP86 functional[38,39] is suitable to predict the infrared spectra of Si_nV^+ and Si_nCu^+ ($n = 6-11$), but the hybrid B3LYP[40-42] better predicts the fragmentation paths.[13] For Mn-compounds the situation is even more complicated. Most available DFT methods fail in reproducing the singlet ground state of Mn_2, although they give relatively good results for magnetic properties of larger Mn clusters.[43]

The configurational space of the doped silicon clusters is rather complex and we have tested systematically a lot of possible structures for each cluster size. In particular, all the structures from our previous studies on V and Cu doped Si clusters and those available in the literature for other dopants are taken as initial configurations. In addition, a large number of initial structures are generated by changing the position of the dopant in a previously located isomer, or by adding Si atoms to the smaller Mn-doped cluster, or by removing Si atoms from the larger one. If an initial shape relaxes to two different structures for two electronic spin states, we take the new structure of the other spin state for further optimizations.

We have extensively tested several DFT functionals including BP86, B3LYP, B3P86, and M06.[44] So far, the BP86 and B3LYP functionals are the most common choices to access the geometrical and electronic structures of transition metal compounds. The less commonly used B3P86 functional,[39,42] composed of Becke's hybrid 3-parameter exchange and the P86 non-local correlation, has the same percentage of the exact Hartree-Fock exchange (20%) as B3LYP. The new-generation meta-hybrid M06 functional was fitted on a data set including both transition metals and non-metals.[44]

The performance of the chosen functionals has been initially tested for Si_6Mn^+. The different functionals give the same predictions for the (putative) ground state which is a pentagonal bipyramid with the Mn situated at the equatorial position in a quintet electronic state. Figure 1 shows that the IRMPD spectrum of Si_6Mn^+ can be much better reproduced with the ground state's vibrational spectrum calculated by the B3P86 functional than when using the other considered functionals. The BP86 and

M06 functionals do not reproduce the amount of peaks observed in experiment. The B3LYP functional does not predict the peak positions well.

Another situation occurs for Si_7Mn^+: the pure functional BP86 predicts a singlet ground state while the hybrid functionals (B3P86, B3LYP, and M06) predict high-spin ground states (quintet or septet). The two 3-parameter hybrid functionals B3P86 and B3LYP have similar high-low spin state energy differences, but the M06 predicts much higher energies for the low spin states (singlet and triplet). These differences are also observed for the larger cluster sizes Si_8Mn^+, Si_9Mn^+, and $Si_{10}Mn^+$. This is due to the fact that the percentage of exact Hartree-Fock exchange in M06 is larger than that in B3LYP and B3P86.

The difficulty in predicting the ground states of Si_nMn^+ as compared to the other doped silicon clusters may relate to the high spin character of Mn. The failure of the pure BP86 functional in reproducing high spin states can be rationalized by the sizable spurious self-interaction of localized Mn 3*d*-states.[45] This self-interaction leads to over-delocalization of 3*d*-states and enhances the overlap of Mn 3*d* and 4*s* orbitals, which in turn causes an underestimation of the *s*-*d* promotion energy. Therefore, a hybrid functional containing an appropriate portion of exact Hartree-Fock exchange, which is self-interaction-free, can better describe the localized Mn 3*d*-states.[46] The fact that the B3P86 functional reproduces the IR spectra better without scaling is due to a mutual compensation of an underestimation of the vibrational frequencies using the pure BP86 functional by a typical overestimation of the Hartree-Fock component. Other hybrid functionals (B3LYP and M06) fail in predicting the vibrational spectra, which implies that the B86 correlation functional outperforms other functionals in this respect. Overall, we find that the hybrid B3P86 functional is superior to the other functionals considered in reproducing the IRMPD spectra of the Si_nMn^+ clusters with the computed IR spectra of the identified lowest energy structure. The results reported hereafter are therefore obtained using the B3P86 functional in combination with the 6-311+G(d) basis set.[47] All the calculations are performed using the Gaussian 03

package.[48] Magnetic moments, atomic charges, and electron distribution are evaluated based on natural population analysis which is performed at the same level of theory using the NBO 5.G program.[49] The calculated line spectra are folded with a Gaussian line width function of 3 or 5 cm^{-1} full width at half maximum (FWHM). The value of the FWHM is chosen to be close to the broadening that is expected by the FELIX bandwidth of typically 0.5−1 % FWHM.

3. Results and Discussion

A. Structural Identification

The IRMPD spectra of the $Si_nMn^+ \cdot RG$ species, in which *RG* is Ar for n = 6, 8−10 and Xe for n = 7, 11−14, 16, are given in Figures 2 and 3. For n = 6, 9, and 10, IRMPD spectra are recorded for $Si_nMn^+ \cdot Xe$ in addition and are very similar to the corresponding $Si_nMn^+ \cdot Ar$ spectra (see the Electronic Supplementary Information, ESI). We do not discuss the structural identification of $Si_{11}Mn^+$ and $Si_{15}Mn^+$. For $Si_{11}Mn^+$, the experimental IRMPD spectrum could be recorded, but no match with the obtained low-energy isomers has been found. So most likely, we have not found the isomers responsible for the IR spectrum of this cluster. The IRMPD spectrum of $Si_{15}Mn^+ \cdot Xe$ could not be recorded due to the mass coincidence of $Si_{15}Mn^+$ and $Si_{13}Mn_2^+$ in combination with a high abundance of $Si_{13}Mn_2^+$ in the cluster beam.

The calculated harmonic vibrational spectra of the isomers that fit the experimental IRMPD spectra best are included in Figures 2 and 3. For the small clusters with n = 6-10, which are shown to contain exohedral Mn atoms, the assignment appears more certain (Figure 2) than for the larger sizes (Figure 3). The assigned isomers correspond to the lowest-lying isomers located, except for Si_8Mn^+ where the second lowest-lying isomer matches the experimental finding best, but this isomer is only 0.02 eV above the computed ground state; the two isomers can be regarded as energetically degenerate.

For Si_6Mn^+ we identify a C_{2v} pentagonal bipyramidal structure in a $^5B_2$ state, similar to the

structure of the Si_6V^+ cluster,[13,32] but the local magnetic moment on the Mn (4.3 μ_B) is much higher than that on the V atom (2.5 μ_B). A $^7B_2$ state possessing the same structure and lying 0.39 eV higher than the $^5B_2$ state has a similar infrared spectrum (see ESI) and possibly might also contribute to the experimental spectrum.

The structure of Si_7Mn^+ is an edge-capped pentagonal bipyramid, similar to the structure of Si_8^+,[3] with a high spin $^7A_1$ ground state. The Mn atom in this isomer caps an equatorial edge of the pentagonal Si_7, and has a local magnetic moment of 5.7 μ_B which is close to that of the isolated Mn^+ cation (6 μ_B).

For Si_8Mn^+, several isomers are located within only 0.1 eV, however, a C_s bicapped pentagonal bipyramid being 0.02 eV above the lowest-lying isomer, where the Mn atom is incorporated in the pentagon, is assigned upon comparison with experiment. The Mn center possesses a local magnetic moment of 4.2 μ_B, which is similar to that in Si_6Mn^+ and has the same coordination number. Based on the comparison with the IRMPD spectrum of Si_8Mn^+·Ar (see ESI), it is concluded that the lowest-lying isomer found for Si_8Mn^+ at the B3P86 level is not significantly contributing to the experimental spectrum.

Si_9Mn^+ is a distorted tetracapped trigonal prism in which Mn substitutes a Si atom of the prism, and has a quintet state. The corresponding C_s structure lying at 0.27 eV above the distorted one is a transition state. Although the Mn atom in Si_9Mn^+ has a higher coordination number than in the smaller sizes, it still possesses a large local magnetic moment of 4.2 μ_B. The second low-lying isomer, being 0.01 eV higher in energy than the lowest-lying isomer and having a tricapped pentagonal bipyramid shows a similar vibrational spectrum (see ESI). It can therefore not be excluded that this isomer is (also) present in the molecular beam.

$Si_{10}Mn^+$ is a C_s pentacapped trigonal prism, similar to the structure of Si_{11}^+,[3] with a $^5A'$ state. This cluster can be formed by adding the Mn on a face of the Si_{10} tetracapped trigonal prism and also

carries a large local magnetic moment of 4.4 μ_B.

For doped silicon clusters composed of at least twelve silicon atoms, endohedral clusters, which are theoretically predicted to be low in energy, are assigned on the basis of the comparison of vibrational spectra. However, we are not always able to obtain a conclusive assignment as shown in Figure 3 where the IRMPD spectra of some cluster sizes are better interpreted by calculated spectra of more than one low-lying isomer.

A ^3A_g lowest-energy state of the hexagonal prism (C_i symmetry) is found for $Si_{12}Mn^+$. The local magnetic moment on the Mn center amounts to 1.6 μ_B. The ^1A_g state with a D_{6h} symmetric hexagonal prism is 0.41 eV higher in energy than the corresponding triplet state. In addition, the presence of this singlet state can be ruled out due to the mismatch between the spectra. This implies that the electronic structure of $Si_{12}Mn^+$ is very different from the isoelectronic $Si_{12}Cr$, for which a singlet state is predicted.[25]

An endohedral distorted capped hexagonal prism (C_{3v} symmetry) is assigned for $Si_{13}Mn^+$ in a low-spin $^1A_1$ configuration with a local magnetic moment on the Mn atom of zero.

No definitive assignment of the structure of $Si_{14}Mn^+$ could be made. The three lowest-lying isomers are a fullerene-like[50] cage with a $^1A_1$' state as the lowest energy isomer (**D_{3h}**), a $^3A_1$ state having similar structure (**C_{2v}**) lying at 0.30 eV higher in energy, and a bicapped hexagonal prism in a triplet state (C_1, 0.13 eV). Each of them has computed IR spectra that show some, but inconclusive, agreement with experiment.

Upon comparison of the IR spectra, we find that three low-lying isomers of $Si_{16}Mn^+$, i.e. the singlet (^{1}A', 0.06 eV), triplet (^{3}A", 0.0 eV), and quintet (^{5}A, 0.23 eV) states of a fullerene-like structure having six pentagonal and two square-like faces are all consistent with the experimental one. Among them, the quintet state, whose Mn atom possesses a local magnetic moment of 2.4 μ_B, appears to

reproduce the experimental spectrum best. Nonetheless, because of the limited quality of the experimental spectrum, no definitive conclusion can be drawn.

B. Magnetism

The most remarkable property of the studied Si_nMn^+ clusters is the high spin ground states of the exohedral, and to a lesser extent of the endohedral clusters. This magnetic behavior has not been found in silicon clusters that are exohedrally doped with other 3*d* TMs such as Si_nV^+ and Si_nCu^+ ($n \geq 4$),[13,15] Si_nCr ($n \geq 8$),[19,20] Si_nFe ($n \geq 9$),[21] Si_nCo ($n \geq 7$),[22] Si_nNi ($n \geq 3$),[23] or even neutral Si_nMn ($n \geq 8$).[33] In the present work, the Mn center is found to possess a local spin magnetic moment of 5.6 μ_B in Si_7Mn^+, while it amounts to 4.2−4.3 μ_B for the other sizes (n = 6, 8−10) according to the natural population analysis. The atomic charges on the Mn atom are found to be around +1 *e* for all the considered clusters. The number of electron is around 0.3 *e* on the 4*s* shell and 5.6 *e* on the 3*d* shell of Mn for most of sizes, with an exception for Si_7Mn^+ where both the 4*s* and the 3*d* shells are half-filled.

The magnetic moments of the endohedral Mn-doped Si clusters are lower than those of the exohedral ones. This can be understood by the fact that in going from small to larger cluster sizes, the cages are getting large enough to encapsulate the dopant atom, but then the orbitals of the cage have more *d*-character which facilitates the stabilizing interaction with the unpaired 3*d* orbitals of the Mn. Nevertheless, the magnetic properties of the large Si_nMn^+ clusters turn out to be special as compared with those of other dopants encapsulated in silicon cages.[24-26] In particular, we obtain triplet ground states for $Si_{12}Mn^+$ and $Si_{16}Mn^+$, and find several quintet states at relatively low energies relative to the corresponding lowest-lying states. This behavior is stemming from the special electronic state of the Mn atom, with a relatively stable $3d^5$ shell, causing a higher resistance to the overlap with the cage's orbitals as compared with other transition metal dopants.

Figure 4 illustrates the evolution of the lowest relative energy (in eV) of each spin state (singlet, triplet, quintet or septet) versus the cluster size (*n*) at the B3P86/6-311+G(d) level of theory. The singlet

states (blue rhombuses) are found to be very high in energy for smaller sizes but become favorable with increasing size. The triplet states (red squares) stay low in energy for most sizes. The quintet states (green triangles) are favored for the small clusters but are higher in energy for intermediate sizes. For n=16 the quintet becomes competitive again and singlet and triplet are nearly degenerate. In contrast to the singlet states, the septet states of exohedral clusters are comparably low in energy while those of endohedral clusters are the energetically highest states. Considering the magnetic property, the high spin states in the low-energy region make the Si_nMn^+ clusters of potential interest for nanostructured materials with tuned local magnetic moments.

C. Growth Mechanism

Structurally, all of the small Si_nMn^+ clusters (up to n = 10) can markedly be described as substitution derivatives of the bare Si_{n+1}^+ cations[3] (see Figure 2), and this occurs in spite of the very different electronic nature of Si and Mn. The high magnetic moment found for all exohedral Si_nMn^+ clusters investigated here represents a particular property in view of the low magnetic moment for both interstitial and substitutional manganese atoms in bulk silicon crystals.[31]

Similar to other transition metals in the 3*d* row,[25] the Mn atom can be encapsulated in a Si_{12} hexagonal prism cage but bearing a triplet state instead of the singlet state or doublet found for the other TM dopants. When compared to $Si_{13}V^+$, $Si_{13}Mn^+$ also exhibits a top-capped hexagonal prism structure but with some distortion, which induces square-like faces instead of triangular faces in $Si_{13}V^+$.[24] Subsequently, a fullerene-like structure, which is composed of square-like and pentagonal faces, is formed for $Si_{14}Mn^+$, instead of the bicapped hexagonal prism found for $Si_{14}V^+$.[24] Also for $Si_{16}Mn^+$, fullerene-like structures with pentagonal and square faces are favored. The less compact fullerene-like structures of the endohedral Si_nMn^+ clusters significantly differ from the more compact structures found for Si_nV^+.[24]

4. Conclusions

In conclusion, our combined experimental and theoretical study allows the structures of manganese doped silicon clusters Si_nMn^+ (n = 6−10, 12−14, 16) to be identified and their IR spectra to be assigned. In most cases, the spectra of the lowest energy isomers found using the B3P86 hybrid functional basically reproduce the experimental IRMPD spectra. The exohedral Mn-doped silicon clusters are found to have unusually high magnetic moments, which are mainly localized on Mn, namely, ~6 μ_B for Si_7Mn^+ and ~4 μ_B for the other sizes. The structures of Si_nMn^+ with n = 6−10 are consistently similar to those of the bare Si_{n+1}^+ cations with the Mn atom located at a low coordinated position. The substitution behavior of Mn and the high magnetic moments conserved in the exohedral Si_nMn^+ clusters suggest that the Mn atom is a magnetic copy of the Si in the Si_{n+1}^+ clusters. The endohedral Mn-doped silicon clusters tend to favor fullerene-like structures and exhibit energetically accessible higher spin states. Based on this observation, we conjecture that the manganese doped silicon clusters are valuable candidates to be used as building blocks in magnetic nanostructured materials.

Acknowledgements.

We gratefully acknowledge the support of the Stichting voor Fundamenteel Onderzoek der Materie (FOM) in providing beam time on FELIX and highly appreciate the skillful assistance of the FELIX staff. This work is supported by the European Community's *FP7*/2007-2013 (grant n.°226716), the Research Foundation-Flanders (FWO), the Flemish Concerted Action (GOA), the Belgian Interuniversity Poles of Attraction (IAP), and the Deutsche Forschungsgemeinschaft within FOR 1282 (FI 893/4-1). V.T.N thanks KU Leuven for a postdoctoral fellowship, P.C. is grateful for financial support by the Flemish Agency for Innovation by Science and Technology (IWT).

SUPPLEMENTARY INFORMATION AVAILABLE: (1) Selection of the best performing functional

for Si_nMn^+ by comparison with the IRMPD spectra of Si_6Mn^+ and Si_7Mn^+, $Si_{12}Mn^+$ and (2) Structures and vibrational spectra of low-lying Si_nMn^+ (n = 8 - 10, 11, 12 - 14, 16) isomers.

REFERENCES:

1) K. Raghavachari, V. Logovinsky, *Phys. Rev. Lett.* **1985**, *55*, 2853-2856.

2) K.-M. Ho, A. A. Shvartsburg, B. Pan, Z.-Y. Lu, C.-Z. Wang, J. G. Wacker, J. L. Fye, W. L. Brown, *Nature* **1998**, *392*, 582-585.

3) J. T. Lyon, P. Gruene, A. Fielicke, G. Meijer, E. Janssens, P. Claes, P. Lievens, *J. Am. Chem. Soc.* **2009**, 131, 1115-1121.

4) V. Kumar, *Comp. Mat. Sci.* **2006**, *36*, 1-11.

5) H. Hiura, T. Miyazaki, T. Kanayama, *Phys. Rev. Lett.* **2001**, *86*, 1733-1736.

6) S. M. Beck, *J. Chem. Phys.* **1987**, *87*, 4233-4234.

7) F. Hagelberg, C. Xiao, W. A. Lester Jr, *Phys. Rev. B* **2002**, *66*, 035426.

8) J. U. Reveles, S. N. Khanna, *Phys. Rev. B.* **2005**, *72*, 165413.

9) K. Koyasu, M. Akutsu, M. Mitsui, A. Nakajima, *J. Am. Chem. Soc.* **2005**, *127*, 4998-4999.

10) J. B. Jaeger, T. D. Jaeger, M. A. Duncan, *J. Phys. Chem. A* **2006**, *110*, 9310-9314.

11) M. B. Torres, E. M. Fernández, L. C. Balbás, *Phys. Rev. B* **2007**, *75*, 205425.

12) J. T. Lau, K. Hirsch, Ph. Klar, A. Langenberg, F. Lofink, R. Richter, J. Rittmann, M. Vogel, V. Zamudio-Bayer, T. Möller, B. v. Issendorff, *Phys. Rev. A.* **2009**, *79*, 053201.

13) V. T. Ngan, P. Gruene, P. Claes, E. Janssens, A. Fielicke, M. T. Nguyen, P. Lievens, *J. Am. Chem. Soc*. **2010**, *132*, 15589-15602.

14) E. Janssens, P. Gruene, G. Meijer, L. Wöste, P. Lievens, A. Fielicke, *Phys. Rev. Lett.* **2007**, *99*, 063401.

15) P. Gruene, A. Fielicke, Meijer, G.; E. Janssens, V. T. Ngan, M. T. Nguyen, P. Lievens, *ChemPhysChem* **2008**, *9*, 703-706.

16) A.-H. Lu, E. L. Salabas, F. Schüth, *Angew. Chem.* **2007**, *119*, 1242-1260.; *Angew. Chem. Int. Ed.* **2007**, *46*, 1222-1244.

17) S. A. Wolf, D. D. Awschalom, R. A. Buhrman, J. M. Daughton, S. von Molnar, M. L. Roukes, A. Y. Chtchelkanova, D. M. Treger, *Science* **2001**, *294*, 1488-1495.

18) A. Grubisic, Y. J. Ko, H. Wang, K. H. Bowen, *J. Am. Chem. Soc.* **2009**, *131*, 10783-10790.

19) H. Kawamura, V. Kumar, Y. Kawazoe, *Phys. Rev. B* **2004**, *70*, 245433.

20) S. N. Khanna, B. K. Rao, P. Jena, *Phys. Rev. Lett.* **2002**, *89*, 016803.

21) L. Ma, J. Zhao, J. Wang, B. Wang, Q. Lu, G. H. Wang, *Phys. Rev. B* **2006**, *73*, 125439.

22) J. Wang, J. Zhao, L. Ma, B. Wang, G. Wang, *Phys. Lett. A* **2007**, *367*, 335-344.

23) J. Li, C. Yao, Y. Mu, J. Wan, M. Han, *J. Mol. Struct.: Theochem* **2009**, *916*, 139-146.

24) P. Claes, E. Janssens, V. T. Ngan, P. Gruene, J. T. Lyon, D. J. Harding, A. Fielicke, M. T. Nguyen, P. Lievens, *Phys Rev Lett* **2011,** *107*, 173401.

25) P. Sen, L. Mitas, *Phys. Rev. B* **2003**, *68*, 155404.

26) E. N. Koukaras, C. S. Garoufalis, A. D. Zdetsis, *Phys. Rev. B* **2006**, *73*, 235417.

27) A. K. Singh, T. M. Briere, V. Kumar, Y. Kawazoe, Phys. *Rev. Lett.* **2003,** *91*, 146802.

28) R. Robles, S. N. Khanna, *Phys. Rev. B* **2009**, *80*, 115414.

29) M. Cheeseman, R. J. Van Zee, H. J. Flanagan, W. Weltner Jr, *J. Chem. Phys.* **1990**, *92*, 1553.

30) J. Shi, J. M. Kikkawa, R. Proksch, T. Schaffer, D. D. Awschalom, G. Medeirosribeiro, P. M. Petroff, *Nature* **1995**, *377*, 707-710.

31) X. Zhang, M. Brynda, R. D. Britt, E. C. Carroll, D. S. Larsen, A. I. Louie, S. M. Kauzlarich, *J. Am. Chem. Soc.* **2007**, *129*, 10668-10669.

32) G. W. Ludwig, H. H. Woodbury, *Solid State Phys.* **1962**, *13*, 223-304.

33) J. Li, G. H. Wang, C. H. Yao, Y. W. Mu, J. G. Wan, M. Han, *J. Chem. Phys.* **2009**, *130*, 164514.

34) W. Bouwen, P. Thoen, F. Vanhoutte, S. Bouckaert, F. Despa, H. Weidele, R. E. Silverans, P. Lievens, *Rev. Sci. Instrum.* **2000**, *71*, 54.

35) A. Fielicke, G. von Helden, G. Meijer, *Eur. Phys. J. D* **2005**, *34*, 83.

36) D. Oepts, A. F. G. van der Meer,; P. W. van Amersfoort, *Infrared Phys. Technol.* **1995**, *36*, 297

37) K. R. Asmis, A. Fielicke, G. von Helden, G. Meijer, *Atomic Clusters: From Gas Phase to Deposited*, *edited by D. P. Woodruff, Elsevier, Amsterdam*, **2007**, p.327.

38) A. D. Becke, *Phys. Rev. A* **1988**, *38*, 3098-3100;

39) J. P. Perdew, *Phys. Rev. B* **1986**, *33*, 8822-8824.

40) C. Lee, W. Yang, R. G. Parr, *Phys. Rev. B* **1988**, *37*, 785-789.;

41) B. Miehlich, A. Savin, H. Stoll, H. Preuss, *Chem. Phys. Lett.* **1989**, *157*, 200;

42) A. D. Becke, *J. Chem. Phys.* **1993**, *98*, 5648.

43) M. Kabir, A. Mookerjee, D. G. Kanhere, *Phys. Rev. B* **2006**, *73*, 224439.

44) Y. Zhao, D. G. Truhlar, *Theor. Chem. Acc.* **2008**, *120*, 215-241.

45) S. Kümmel, L. Kronik, *Rev. Mod. Phys.* **2008**, *80*, 3-60.

46) A. Stroppa, G. Kresse, A. Continenza, *Phys. Rev. B* **2011**, 83, 085201.

47) A. J. H. Wachters, *J. Chem. Phys.*, **1970**, 52, 1033; P. J. Hay, *J. Chem. Phys.* **1977**, 66, 4377.

48) Gaussian 03, Revision C.02, M. J. Frisch, et *al*., Gaussian, Inc., Wallingford CT, **2004**.

49) E. D. Glendening, et al., NBO 5.G. **2004** (Theoretical Chemistry Institute, University of Wisconsin, Madison, WI).

50) T. Miyazaki, H. Hiura, T. Kanayama, *Phys Rev B* **2002,** *66*, 121403.

FIGURE CAPTIONS:

Figure 1. The IR spectra of the Si_6Mn^+ lowest energy states as obtained using four different functional (B3P86, BP86, B3LYP, and M06) in comparison with the experimental IRMPD spectrum of Si_6Mn^+·Ar (upmost panel). The red crosses are the original data points, while the full line corresponds to a three point running average. The *y*-axis is in km/mol for the theoretical infrared intensities and has arbitrary units for the IRMPD experiment.

Figure 2. IRMPD spectra of Si_nMn^+·*RG* (*RG* = Ar for $n = 6$, 8−10 and *RG* = Xe for $n = 7$) and the corresponding calculated harmonic vibrational spectra of the best fitting isomers. The red crosses are the original data points, while the full line corresponds to a three point running average. The *y*-axis is in km/mol for the theoretical infrared intensities and has arbitrary units for the experiment. The assigned structures are illustrated to the right of the corresponding spectra together with their electronic states. The ground state structures of Si_{n+1}^+ (taken from ref. 3) are given next to them for comparison.

Figure 3. IRMPD spectra of Si_nMn^+·Xe ($n = 11-14$, 16) are presented in the upmost trace for each cluster size; the red crosses are the original data points, while the full line corresponds to a three point running average. The corresponding calculated harmonic vibrational spectra of the assigned low-lying isomers are given below the experimental traces. The electronic states and relative energies (in eV) of the isomers are given. The *y*-axis is in km/mol for the theoretical infrared intensities and has arbitrary units for the experiment. The structures are illustrated to the right of the corresponding spectra.

Figure 4. Plot of the relative energies (eV) of the lowest-energy isomer found for Si_nMn^+ at the B3P86/6-311+G(d) level for each spin state (singlet, triplet, quintet septet) as function of the cluster size ($n = 6-10$, 12−14, and 16).

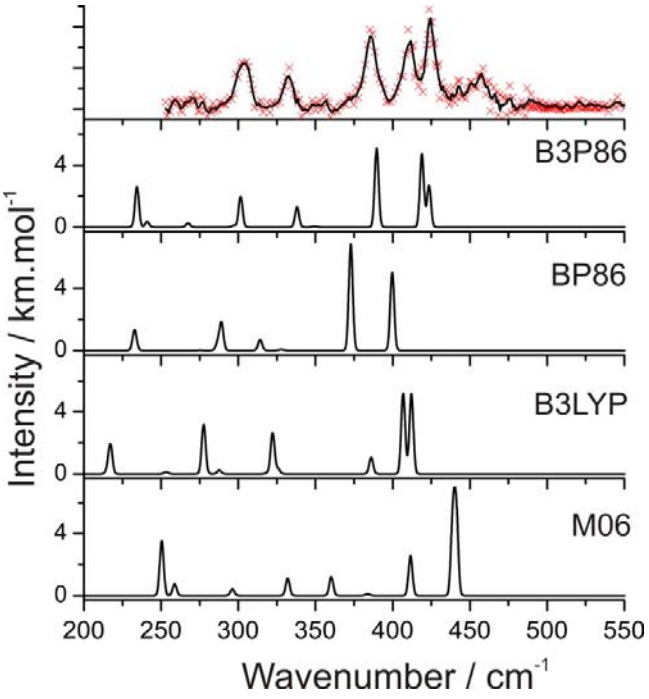
B3P86
BP86
B3LYP
M06
Intensity / km.mol-1
Wavenumber / cm-1
0
4
200
250
300
350
400
450
500
550

Figure 1

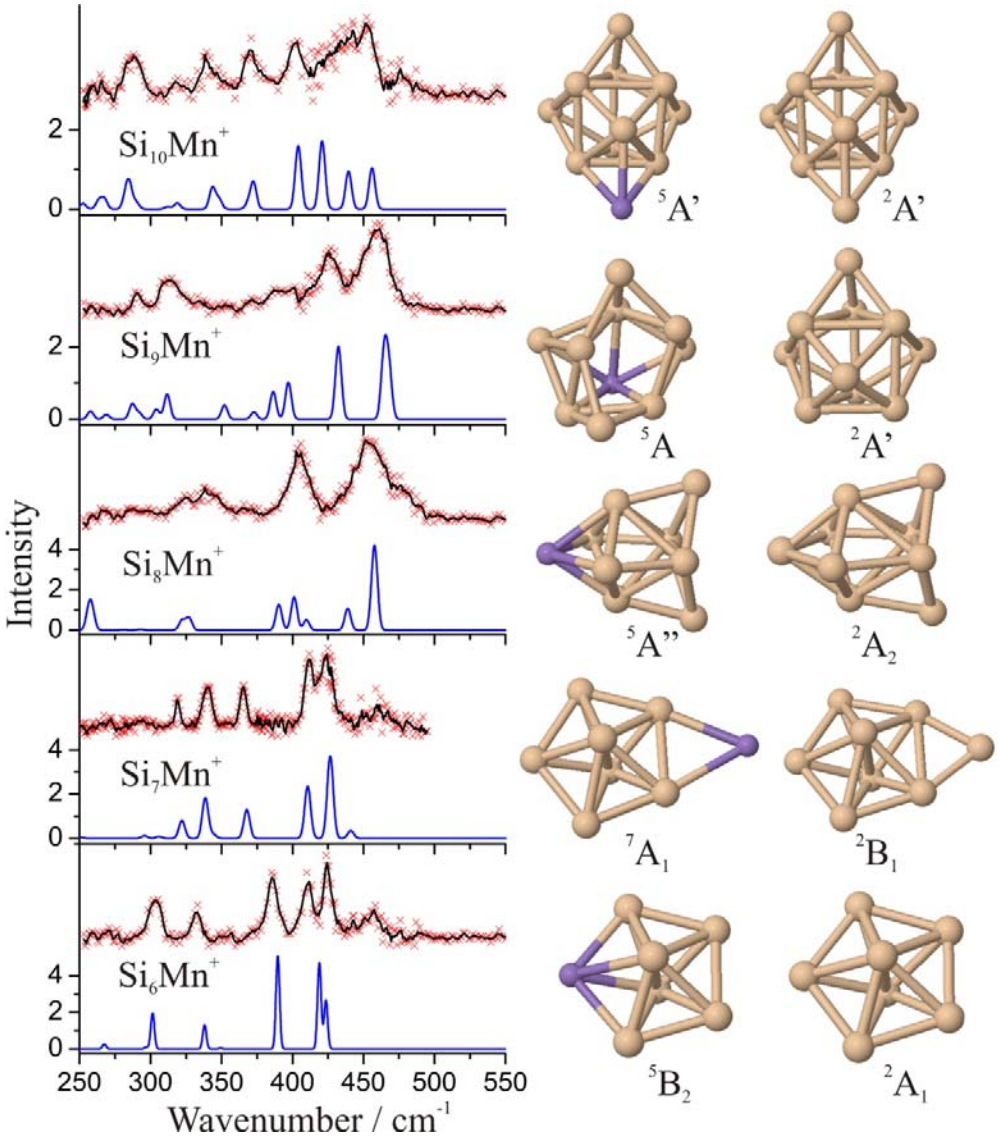
Intensity
Si10Mn+
Si9Mn+
Si8Mn+
Si7Mn+
Si6Mn+
Wavenumber / cm-1
5A'
2A'
5A
2A'
5A"
2A2
7A1
2B1
5B2
2A1

Figure 2

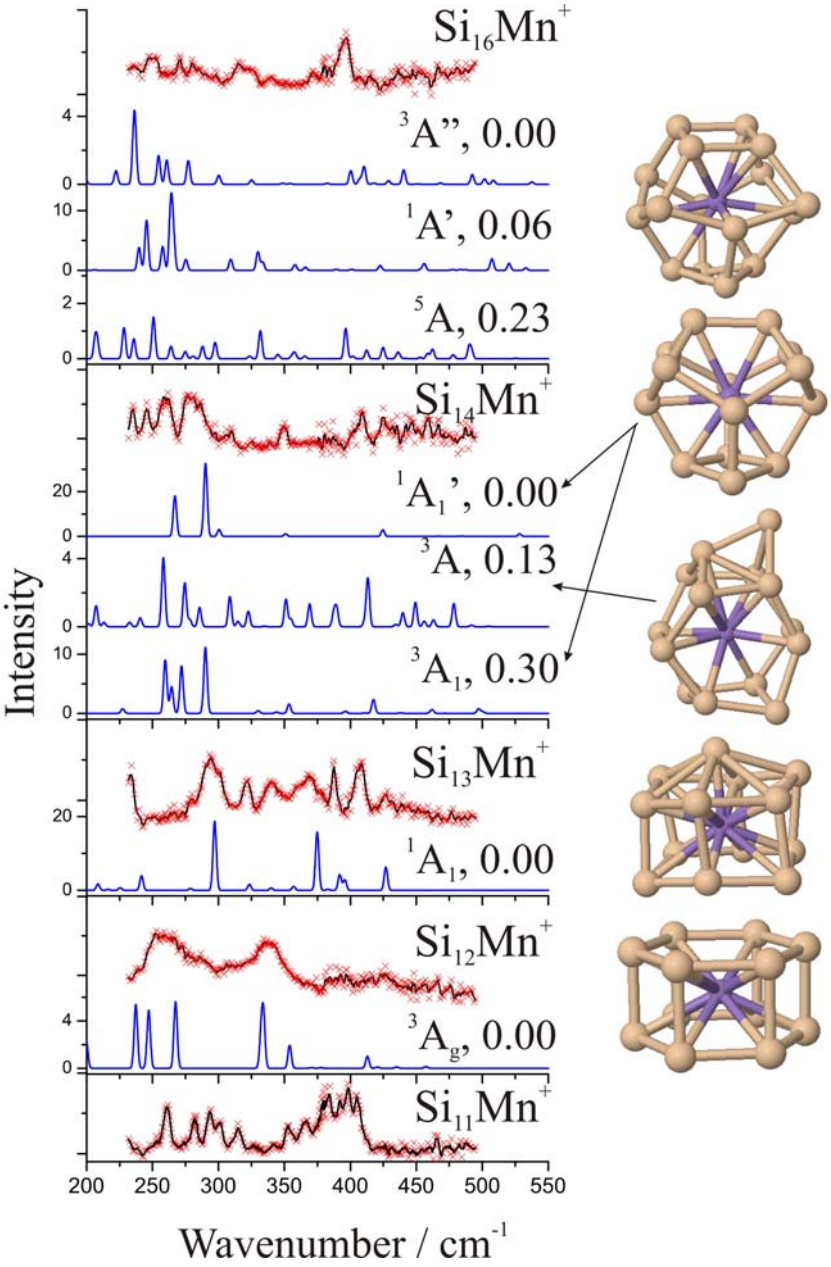
Si16Mn+
3A", 0.00
1A', 0.06
5A, 0.23
Si14Mn+
1A1', 0.00
3A, 0.13
3A1, 0.30
Si13Mn+
1A1, 0.00
Si12Mn+
3Ag, 0.00
Si11Mn+
Intensity
200 250 300 350 400 450 500 550
Wavenumber / cm-1

Figure 3

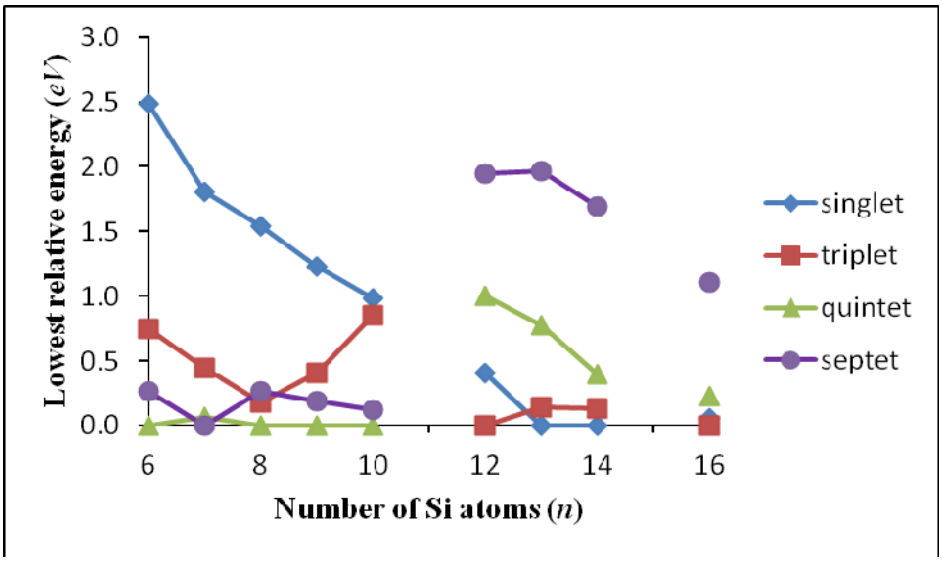
Lowest relative energy (eV)
3.0
2.5
2.0
1.5
1.0
0.5
0.0
6
8
10
12
14
16
Number of Si atoms (n)
singlet
triplet
quintet
septet

Figure 4

TABLE OF CONTENT